

# Universal nonlinear stage of the locally induced modulational instability in fiber optics

Adrien E. Kraych,<sup>1</sup> Pierre Suret,<sup>1</sup> Gennady El,<sup>2</sup> and Stéphane Randoux<sup>1,\*</sup>

<sup>1</sup>Univ. Lille, CNRS, UMR 8523 - PhLAM - Physique des Lasers Atomes et Molécules, F-59000 Lille, France

<sup>2</sup>Department of Mathematical Sciences, Loughborough University, Loughborough LE11 3TU, United Kingdom

(Dated: May 15, 2018)

We report an optical fiber experiment in which we study nonlinear stage of modulational instability of a plane wave in the presence of a localized perturbation. Using a recirculating fiber loop as experimental platform, we show that the initial perturbation evolves into expanding nonlinear oscillatory structure exhibiting some universal characteristics that agree with theoretical predictions based on integrability properties of the focusing nonlinear Schrödinger equation. Our experimental results demonstrate persistence of the universal evolution scenario, even in the presence of small dissipation and noise in an experimental system that is not rigorously of an integrable nature.

Modulational instability (MI), known as the Benjamin-Feir instability in water waves, is a ubiquitous phenomenon in focusing nonlinear media that is manifested in the growth of small, long-wavelength perturbations of a constant background [1–9]. The linear stage of MI is characterized by an exponential growth of all the perturbations falling in the region of the Fourier spectrum below certain cut-off wavenumber [5]. This simple picture ceases to be valid when the amplitude of the growing perturbation becomes comparable to the background, i.e. at the nonlinear stage of MI.

In the nonlinear regime, MI exhibits a rich spatiotemporal dynamics that has been recently the subject of significant interest in several areas of experimental and theoretical physics [10–19]. In this respect, the focusing one-dimensional nonlinear Schrödinger equation (1D-NLSE) plays a prominent role as a universal mathematical model describing at leading order wave phenomena relevant to many fields of nonlinear physics such as e.g. optics and hydrodynamics [20]. A particular scenario of the MI development strongly depends on the type of initial conditions considered. In the majority of the existing analytical, numerical and experimental studies of MI periodic or random initial modulations of a constant background have been considered [10–13, 17–19, 21]. For these types of initial conditions the nonlinear stage of the MI development was shown to be dominated by breather-like structures such as the Akhmediev, Kuznetsov-Ma, Peregrine breathers and their generalizations. The role of NLSE breather solutions has been extensively discussed in the last years in the context of the formation of rogue waves [22, 23]. A particular type of breather solutions of the 1D NLSE, the so-called superregular solitonic solutions have been shown in [24, 25] to describe the development of a certain type small *localized* perturbations of the plane wave [26].

When a localized (and not necessarily small) initial perturbation of a plane wave has an arbitrary shape (within a reasonably broad class), it was recently shown

using the inverse scattering transform solutions of the 1D-NLSE that the nonlinear dynamics of MI is characterized by a “hyperbolic” scenario, where a universal (not depending on the shape of the initial localized perturbation to leading order) nonlinear oscillatory structure develops and expands in time with *finite speed* [27, 28]. In sharp contrast with the previously mentioned MI scenarios involving the formation of various breathers, this scenario involves the formation of a symmetric expanding nonlinear wave structure described by the modulated elliptic solution of the 1D-NLSE. The modulation provides a gradual transition from a fundamental soliton resting at the center to small-amplitude dispersive waves propagating away from the center with linear group velocity. This universal modulated elliptic solution of the 1D-NLSE saturating the MI was first obtained in [29] in the framework of the Whitham modulation theory [30]. Importantly, considered for either left or right spatial domain (assuming the traditional “mathematical” notions of space and time variables in the 1D-NLSE) this modulation solution was also shown to describe the development of the 1D-NLSE “focusing dam break” problem [15, 31, 32]. This remarkable connection between two apparently unrelated problems provides an additional insight into the nonlinear dynamics of MI.

It has been demonstrated in ref. [33] that the qualitative behaviors found within the integrable NLSE framework are robust and the considered nonlinear stage of MI can also be found in a variety of other wave systems being not necessarily integrable. In view of the fundamental significance of the 1D-NLSE and its generalizations, the experimental realization of this universal scenario of the MI development is of major importance for nonlinear physics.

In this paper, we report the experimental observations of the space-time dynamics of a modulationally unstable plane wave modified by two types of localized, real-valued perturbations: a hump and a well. Using a recirculating fiber loop as experimental platform, the perturbed plane wave is propagated over hundreds of kilometers with only very small power losses. The behaviors observed experimentally are quantitatively very well described by the 1D-NLSE with a small linear damping term, and our ex-

---

\*Electronic address: stephane.randoux@univ-lille1.fr

perimental observations reveal that the wave structure described by the solution considered in ref. [27–29, 31, 33] is robust to noise and to the deviations from integrability that are inherent in any experimental system.

Even though modern single mode fibers (SMFs) represent propagation media with very small linear losses (typically  $\sim 0.2$  dB/km at the telecommunication wavelength of 1550 nm), their attenuation cannot be considered as being fully negligible over propagation distances of a few kilometers. Many of the optical fiber experiments realized those last years for the observation of breather solutions of the 1D-NLSE have encompassed this constraint by using waves with an optical power of the order of  $\sim 1$  Watt. With this power, the characteristic nonlinear length typically ranges between 100 m and 1 km so that single-pass propagation experiments reasonably well described by the 1D-NLSE can be performed within propagation lengths between one to several kilometers. In all single pass fiber geometries where Watt-level powers are required, the generated nonlinear structures have typical durations falling between  $\sim 1$  ps and  $\sim 10$  ps. This requires the use of fast optical detection devices like optical sampling oscilloscopes or time lenses [11, 34–37]. Moreover the observation of the space-time dynamics in single-pass optical fiber experiments often represents a difficult task since it relies on destructive cut-back techniques [38] or alternatively, on nonlinear digital holography methods [39, 40].

In our work, we have adopted another strategy by implementing a recirculating fiber loop that presents the significant advantage to provide real-time observation of the space-time dynamics of the optical wave. Recirculating fiber loops have been previously used under many circumstances in the context of optical fiber communication [41], in particular to demonstrate long-distance transmission of solitons [42–45]. Here this fiber system is used to provide in a non-destructive way the real-time stroboscopic view of the “slow” evolution of the perturbed plane wave, round trip after round trip inside a passive fiber ring cavity. In our recirculating fiber loop, the optical power is kept typically around only  $\sim 10$  mW and the propagation distances that are reached can be as large as hundreds of kilometers. With this experimental approach, all the physically-relevant characteristic lengths and durations are rescaled by one or two orders of magnitude, i.e. the nonlinear length becomes of the order of  $\sim 100$  km and the typical duration of soliton structures becomes  $\sim 50$  ps. With such a time scale, the local perturbation of the plane wave can be relatively easily engineered by using standard fast electro-optic modulators (EOMs). Moreover the detection part can be ensured by fast electronic devices like photodiodes and oscilloscopes.

Our experimental setup is schematically shown in Fig. 1. It consists of a recirculating fiber loop, i.e. a passive ring cavity made up of  $\sim 4$  km of SMF closed on itself by a 90/10 fiber coupler. The coupler is arranged in such a way that 90% of the intracavity power is recirculated. A wide light pulse of  $\sim 100$  ns having a square shape

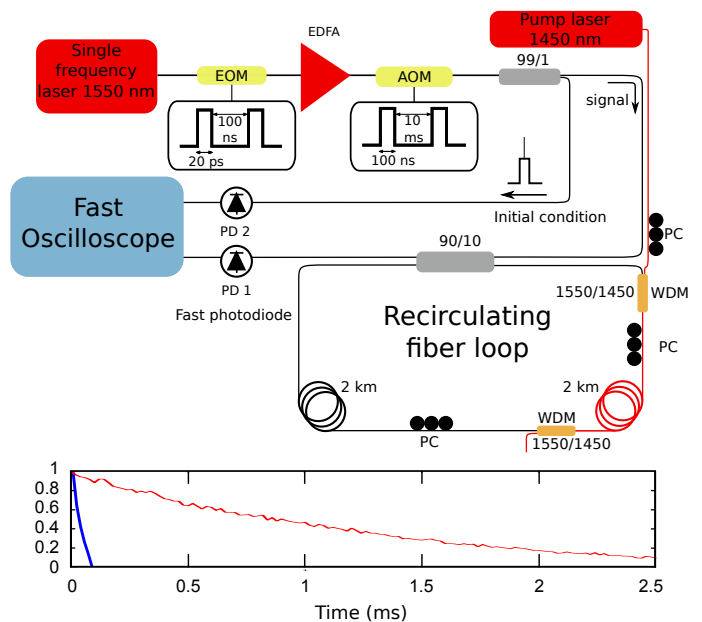


FIG. 1: Schematic representation of the experimental setup. PC: polarization controller, EDFA: Erbium-doped fiber amplifier, AOM: acousto-optic modulator. The bottom part represents the decay of the plane wave measured in absence (blue line) and in presence (red line) of Raman amplification at a pump power of 535 mW.

is perturbed by a small localized perturbation of  $\sim 30$  ps and circulates in the counterclockwise direction inside the fiber loop. The perturbed square pulse is generated by modulating the power of a single-frequency laser operating at 1550 nm, see Appendix A.

The square pulse plays the role of a perturbed plane wave that is periodically injected inside the loop with a period of 10 ms which is much larger than the cavity round-trip time of  $\sim 20$   $\mu$ s. It is monitored by a fast photodiode (PD1) connected to an oscilloscope having an electrical bandwidth of 65 GHz. This photodiode has been carefully calibrated and the optical power of the plane wave launched inside the loop is known with a relative accuracy that is below  $\sim 10\%$ .

The linear losses of the SMF are around  $\sim 0.2$  dB/km. They are partially compensated by Raman amplification in a section of the loop that is 2–km long. Following the method used in ref. [19, 34], a pump beam at 1450 nm is launched in a counterpropagating (clockwise) direction to provide Raman gain with weak relative intensity noise. The pump power  $P_p$  at 1450 nm is typically around  $\sim 500$  mW which is much greater than the power ( $P_0 \sim 10$  mW) of the plane wave circulating inside the loop. The pump radiation at 1450 nm is coupled in and out the fiber loop by using two wavelength dense multiplexers (WDMs). Increasing the power  $P_p$  of the pump beam at 1450 nm from zero to a few hundreds of mW, the decay time of the square pulse that propagates inside the loop and that is measured by the photodiode PD2 at the output of the fiber coupler dramatically increases from

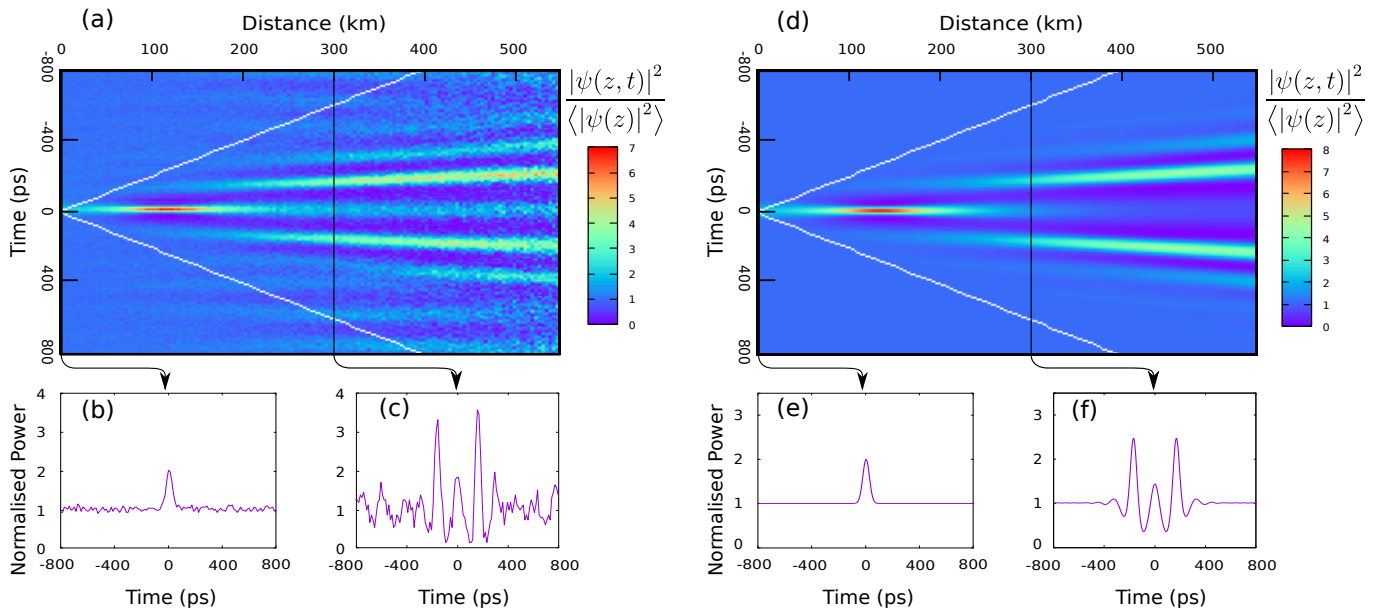


FIG. 2: Space-time evolution of a modulationally-unstable plane wave perturbed at the initial stage by a localized bright (positive) peak. Left part: (a)(b)(c) experiments and right part: (d)(e)(f) numerical simulation of Eq. (1) with  $\beta_2 = -22$  ps<sup>2</sup>km<sup>-1</sup>,  $\gamma = 1.3$ W<sup>-1</sup>km<sup>-1</sup>,  $\alpha_{eff} = 4.2 \times 10^{-3}$  km<sup>-1</sup>,  $P_0 = 14$  mW,  $T_0 = 30$  ps ( $\psi(z=0, t) = \sqrt{P_0}(1 + \exp(-t/T_0)^2)$ ). At each round trip inside the cavity in (a) and (d), the optical power has been renormalized by the mean power carried by the exponentially-decaying plane wave.  $\langle |\psi(z)|^2 \rangle = P_0 \exp(-\alpha_{eff}z)$  represents the mean power of the plane wave at position  $z$ .

$\sim 40$   $\mu$ s to  $\sim 1$  ms, as shown in the bottom part of Fig. 1. Let us emphasize that our ring cavity is conceptually different and also simpler than coherently driven passive cavities used e. g. in ref. [46, 47] as intrinsically bistable devices that can support dissipative cavity solitons.

Fig. 2 (left part) shows the space-time evolution of an optical plane initially perturbed by a localized bright (positive) perturbation having a duration of  $\sim 30$  ps and a peak power twice as large as the mean power (14 mW) of the plane wave, see Fig. 2(b). As shown in Fig. 2(a), the experiment reveals that a nonlinear oscillatory structure develops from the initial localized perturbation and expands with propagation distance, in qualitative agreement with the scenario theoretically described in refs. [27–29, 33]. It should be noted, however, that the structure observed in the experiment captures only the initial stage of the development of MI towards the universal pattern of [27–29, 33, 48] with the fundamental soliton at the center (see Appendix B). Another comment is that a localized perturbation of the plane wave realised in the experiment could generally violate the restriction that the spectrum of the associated scattering problem must be pure continuous required for the analysis in [27, 28]. With the above caveats, the observed pattern confirms the robustness of the universal scenario predicted by the theory.

As discussed in ref.[28], the development of the oscillation behavior of the nonlinear stage of MI under localized perturbations is significantly influenced by noise. Even a very small amount of numerical noise inherent in simulations of the 1D-NLSE with pseudo-spectral methods

significantly perturbs the oscillating structure that is destroyed at finite evolution time [28]. In the experiment, the situation is worse in the sense that (i) the 1D-NLSE only represents an approximate model of the experiment and (ii), the initial plane wave has a non-zero noise level. Therefore, the process of the development of the nonlinear oscillatory structure within the wedge-shaped region of Fig. 2(a) can be completely overtaken by the process of the exponential amplification of the small optical noise that perturbs the laser field at the initial stage.

In our experiment, these difficulties have been circumvented by carefully adjusted the power  $P_0$  of the initial plane wave and the power  $P_p$  of the 1450 nm pump laser. In Fig. 2(a),  $P_0$  and  $P_p$  have been adjusted to 14 mW and 535 mW, respectively. With these values, the growth rate of the oscillatory structure that emerges from the local perturbation, the noise amplification rate and the cavity loss rate are sufficiently well balanced for the nonlinear oscillatory structure to be observed over a propagation distance of  $\sim 500$  km. Any increase of  $P_p$  beyond 535 mW induces some significant amplification of the noise level which results in the destruction of the oscillatory structure generated from the nonlinear evolution of the local perturbation.

Behaviors found in the experiments are retrieved with a good quantitative agreement from the numerical integration of the 1D-NLSE with small linear damping:

$$i \frac{\partial \psi}{\partial z} = \frac{\beta_2}{2} \frac{\partial^2 \psi}{\partial t^2} - \gamma |\psi|^2 \psi - i \frac{\alpha_{eff}}{2} \psi \quad (1)$$

and with parameters corresponding to the experiments.

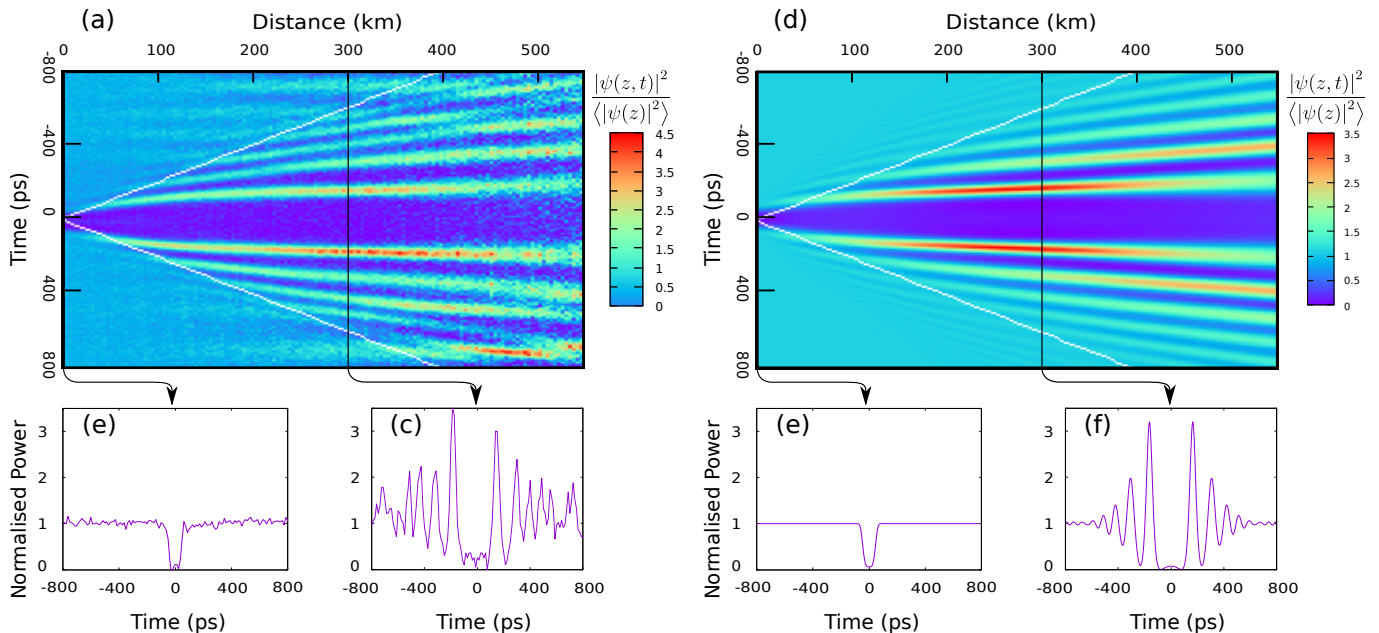


FIG. 3: Space-time evolution of a modulationally-unstable plane wave perturbed at initial stage by a localized dark (negative) peak. Left part: (a)(b)(c) experiments and right part: (d)(e)(f) numerical simulation of Eq. (1) with  $\beta_2 = -22 \text{ ps}^2 \text{ km}^{-1}$ ,  $\gamma = 1.3 \text{ W}^{-1} \text{ km}^{-1}$ ,  $\alpha_{eff} = 4 \times 10^{-3} \text{ km}^{-1}$ ,  $P_0 = 16 \text{ mW}$ ,  $T_0 = 50 \text{ ps}$ ,  $\beta = 0.93$  ( $\psi(z = 0, t) = \sqrt{P_0(1 - \beta \exp(-t/T_0)^4)}$ ).

$\psi(z, t)$  represents the complex envelope of the electric field that slowly varies in space  $z$  and time  $t$ . At 1550nm the group velocity dispersion coefficient of the SMF is  $\beta_2 = -22 \text{ ps}^2/\text{km}$ . The Kerr coefficient is  $\gamma = 1.3 \text{ W}^{-1} \text{ km}^{-1}$  and the effective power losses  $\alpha_{eff}$  measured from the decay rate of the plane wave inside the ring cavity are  $4.2 \times 10^{-3} \text{ km}^{-1}$  (equivalently  $9.6 \times 10^{-4} \text{ dB/km}$ ).

Fig. 2 (right panel) shows the result of the numerical integration of Eq. (1) by taking  $\psi(z = 0, t) = \sqrt{P_0(1 + \exp(-t/T_0)^2)}$  as initial condition. Taking  $P_0 = 14 \text{ mW}$  and  $T_0 = 30 \text{ ps}$ , this expression fits quite well the experimental profile plotted in Fig. 2(b). There is a good quantitative agreement between right (numerical) and left (experimental) parts of Fig. 2, which indeed confirms that our experiment is well described by Eq. (1) where power losses have been introduced in a phenomenological way.

It has been shown in ref. [27, 28] that the development of the oscillation behavior in the nonlinear stage of MI does not depend on the exact shape of the localized perturbation, provided some (relatively mild) conditions necessary for a rigorous treatment are satisfied. We have investigated this point from our experiments. Fig. 3 shows space-time evolution of an optical plane wave initially perturbed by a localized dark (negative) perturbation. Experimental results plotted in the left part of Fig. 3 reveal that a nonlinear oscillatory structure grows from the initial perturbation. One can see that the detailed structure exhibiting two symmetric solitary waves separated by a narrow ‘‘vacuum’’ region in the central part slightly differs from the one observed in the positive

perturbation case. However, the leading order modulation solution describing this structure is the same as in the positive perturbation case. This can be readily understood by noticing that the dynamics of the plane wave under sufficiently negative localized perturbation can be viewed as a combination of two focusing dam breaks of opposite signs located close to each other. It follows from the results of refs. [15, 31, 32] that the modulation solution describing such ‘‘double dam break’’ problem is exactly the same as the one from refs. [27–29, 33] for the positive perturbation case (see Appendix B), confirming the universality of the observed structure.

As shown in the right panel of Fig. 3, the behavior observed experimentally is also quantitatively well described by the numerical simulation of Eq. (1) taking  $\psi(z = 0, t) = \sqrt{P_0(1 - \beta \exp(-t/T_0)^4)}$  as the initial condition ( $P_0 = 16 \text{ mW}$ ,  $\beta = 0.93$ ,  $T_0 = 50 \text{ ps}$ ) that fits the experimental profile shown in Fig. 3(b).

As shown in refs. [27, 29], the boundaries of the region separating the nonlinear oscillatory solution from the plane wave region are expanding linearly with the evolution variable. When rephrased in physical variables, these boundaries are given by  $t_{\pm} = \pm 2\sqrt{2\beta_2\gamma P_0}z$  (see Appendix B). They are plotted with white straight lines in Fig. 2(a)(d) and Fig. 3(a)(d). Even though the oscillatory structure is effectively located within the linear boundaries, the edges of the nonlinear oscillating structure are relatively far from the boundaries predicted by the asymptotic (long-time) theory. This quantitative difference between experiment and theory arises from the fact that the theoretical result has been established in the framework of the purely integrable and *non-dissipative*

1D-NLSE, see Appendix C. Further theoretical work is needed to take into account the influence of a small linear damping term on the mathematical expression giving the boundaries separating the oscillatory region from the plane wave region.

In summary, we have reported an optical fiber experiment in which we have observed the space-time dynamics of a modulationally-unstable plane wave perturbed at initial time by a localized peak. Our experimental results demonstrate the robustness to noise and dissipation of the expanding modulated solution theoretically found in ref. [27–29]. Our experimental platform could be further used to explore some other scenarios of the nonlinear stage of MI, including integrable turbulence or soliton gas [49–52].

### Acknowledgments

This work has been partially supported by the Agence Nationale de la Recherche through the LABEX CEMPI project (ANR-11-LABX-0007), the Ministry of Higher Education and Research, Hauts de France council and European Regional Development Fund (ERDF) through the the Nord-Pas de Calais Regional Research Council and the European Regional Development Fund (ERDF) through the Contrat de Projets Etat-Région (CPER Photonics for Society P4S). The work of GE was partially supported by EPSRC grant EP/R00515X/1. The authors are grateful to Draka-Prysmian for fiber supplying and L. Bigot, R. Habert, E. Andresen and IRCICA-TEKTRONIX European Optical and Wireless Innovation Laboratory for technical support about the electronic devices. The authors are also grateful to A. Musot, C. Naveau and P. Szriftgiser for providing temporary access to some specific optical filter.

### Appendix A: Details of the optical fiber experiment

In this section, we provide more details on the experimental setup sketched in Fig. 1.

The light source used for generation of the plane wave is a single-frequency continuous-wave laser diode (APEX-AP3350A) centered at 1550 nm which delivers an optical power of a few mW. The short localized perturbation of the plane wave is first generated by means of an electro-optic modulator (EOM, NIR-MX-LN series, bandwidth 20 GHz, Photline) driven by an arbitrary waveform generator (AWG70000, bandwidth 50 GHz, Tektronix). The arbitrary waveform generator generates a periodic square electrical signal with a duty cycle of  $2 \times 10^{-4}$ , i.e. the duration of the square electrical pulses is 20 ps and the period of the signal is 100 ns. At the output of the EOM, the light wave has a constant (infinite) background periodically modulated by pulses having a width of 30 ps and a period of 100 ns. The bright (positive) or dark (negative) nature of the peaks modulating the cw background

can be selected by changing the bias voltage applied to the EOM. The contrast of the modulated train of pulses can be varied by changing the control voltage applied to the EOM.

The power of the modulated wave is amplified to the Watt-level by using an Erbium-doped fiber amplifier. Then the amplified wave is optically chopped by an acousto-optic modulator (AOM) that produces a periodic train of square pulses having a width of  $\sim 100$  ns and a period of 10 ms. With this method, we obtain a perturbed plane wave having a duration of  $\sim 100$  ns which is much greater than the typical duration (30 – 50 ps) of the nonlinear structures that are observed. The optical power launched inside the recirculating fiber loop can be adjusted by using a half-wave plate placed before a polarizing cube inside an aerial arm that is not shown in Fig. S1 for the sake of simplicity.

The perturbed square pulse is monitored fast photodiodes (Picometrix D-8IR) connected to a fast oscilloscope (LeCroy Labmaster 10-65ZI) having a bandwidth of 65 GHz and a sampling rate of 80 GSa/s. The photodiode PD1 has been carefully calibrated in some annex experiment and the voltage measured can be converted into optical power with a relative accuracy that is below  $\sim 10\%$ .

The recirculating fiber loop is made up of  $\sim 4$  km of single-mode fiber (SMF) closed on itself by a 90/10 fiber coupler. The coupler is arranged in such a way that 90% of the intracavity power is recirculated. The SMF has been manufactured by Draka-Prysmian. It has a measured second-order dispersion coefficient of  $-22$  ps<sup>2</sup> km<sup>-1</sup> and an estimated Kerr coefficient of  $1.3$  km<sup>-1</sup> W<sup>-1</sup> at the working wavelength of 1550 nm.

Raman amplification is achieved by injecting a pump wave 1450 nm inside the fiber loop. The pump wave is coupled in and out the recirculating fiber loop by using two commercial wavelength dense multiplexers (WDMs) that split light at 1450 nm and at 1550 nm into two separate fiber paths. The distance between the two WDMs inside the recirculating fiber loop is  $\sim 2$  km. The pump laser at 1450 nm is a commercial Raman fiber laser delivering an output beam having a power of several Watt. In our experiments, this optical power is attenuated to typically  $\sim 500$  mW by using a 90/10 fiber coupler (not shown in Fig. 1).

### Appendix B: Modulational instability of a locally perturbed plane wave and the focusing dam break problem

We consider the 1D-NLSE in the form

$$i\varepsilon q_\tau + \frac{1}{2}\varepsilon^2 q_{xx} + |q|^2 q = 0, \quad (\text{B1})$$

where  $\varepsilon$  is the normalized dispersion parameter. The relations between the variables in Eq. (B1) and Eq. (1)

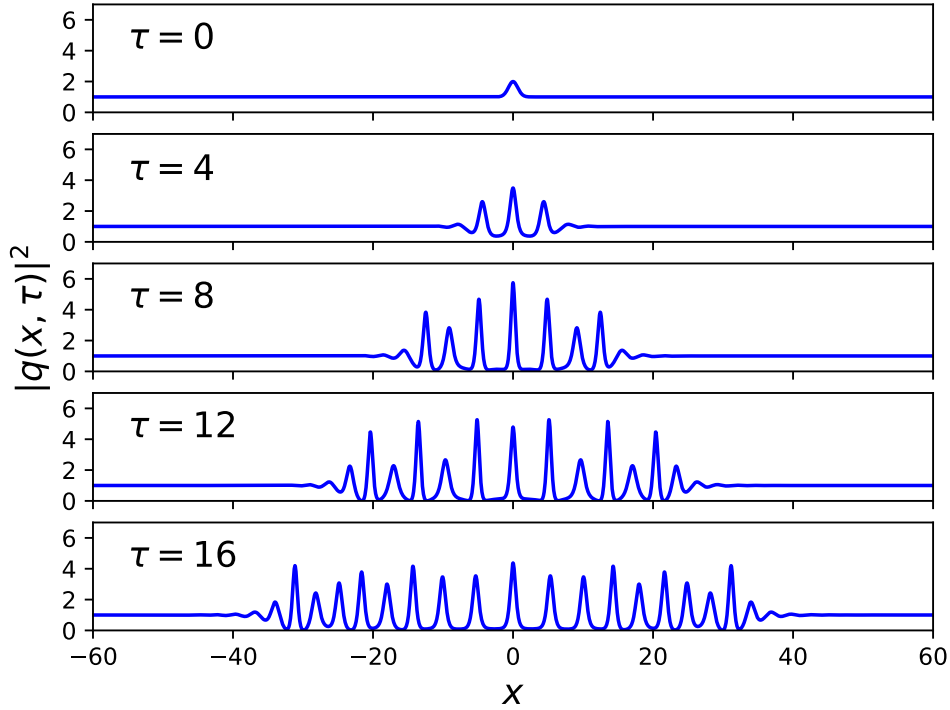


FIG. 4: Evolution of a locally perturbed plane wave towards the universal modulated elliptic wave pattern. Numerical simulation of Eq. (B1) with  $\varepsilon = 1$  and initial data (B3) with  $q_0 = 1$  and  $\delta(x) = (\sqrt{2} - 1) \exp(-x^2)$ . The fiber optics experiment with the positive perturbation reported in Fig. 2 accurately captures the initial stage of the evolution (around  $\tau = 4$ ).

are

$$q = \psi/\sqrt{P_0}, \quad \tau = z/\sqrt{L_{NL}L_D}, \quad x = t/T_P, \quad \varepsilon = \sqrt{L_{NL}/L_D} \quad (\text{B2})$$

where  $T_P$  represents the large initial scale, i.e. the duration of the square pulses in the experiment ( $\sim 100$  ns).  $L_{NL} = 1/(\gamma P_0)$  and  $L_D = T_P^2/|\beta_2|$  represent the nonlinear length and the linear dispersive length, respectively.

We consider Eq. (B1) with the perturbed plane wave initial data

$$q(x, 0) = q_0(1 + \delta(x)), \quad (\text{B3})$$

where  $q_0 > 0$  and  $\delta(x)$  decays sufficiently rapidly as  $|x| \rightarrow \infty$  (see [27, 28] for detailed restrictions on  $\delta(x)$ .)

The *long-time* ( $\tau \gg 1$ ) asymptotic solution of (B1), (B3) was found in [27, 28] to be  $q = Q(x, \tau) +$

$O(1/\sqrt{\tau})$ , where the leading term  $Q(x, \tau)$  has different form in different regions of  $x$ - $\tau$  plane:  $Q(x, \tau) = q_0$  for  $x < -2\sqrt{2}q_0\tau$  and  $x > 2\sqrt{2}q_0\tau$  while for  $x \in [-2\sqrt{2}q_0\tau, 2\sqrt{2}q_0\tau]$  it has the form of slowly modulated travelling wave:

$$|Q(x, t)|^2 = (q_0 + b)^2 - 4q_0b \operatorname{sn}^2 \left( 2\sqrt{q_0b/m} (x - a\tau - x_0)\varepsilon^{-1}; m \right), \quad (\text{B4})$$

where  $\operatorname{sn}(\cdot)$  is a Jacobi elliptic function with the modulus  $m \in [0, 1]$  given by

$$m = \frac{4q_0b}{a^2 + (q_0 + b)^2}.$$

The modulation parameters  $a(x, \tau)$ ,  $b(x, \tau)$  are found from equations

$$\begin{aligned} a &= \sigma \frac{2q}{m\mu(m)} \sqrt{(1-m)[\mu^2(m) + m - 1]}, & b &= \frac{q}{m\mu(m)} [(2-m)\mu(m) - 2(1-m)], \\ \frac{x}{\tau} &= \sigma \frac{2q}{m\mu(m)} \sqrt{(1-m)(\mu^2(m) + m - 1)} \left( 1 + \frac{(2-m)\mu(m) - 2(1-m)}{\mu^2(m) + m - 1} \right), \end{aligned} \quad (\text{B5})$$



where  $\sigma = \text{sgn}(x)$  and  $\mu(m) = E(m)/K(m)$ , where  $K(m)$  and  $E(m)$  are the complete elliptic integrals of the first and second kind respectively. The initial phase  $x_0$  in (B4) depends on the specific form of the perturbation function  $\delta(x)$ . The modulated elliptic solution (B4), (B5) was originally obtained in [29] in the framework of the Whitham modulation theory [30], where the universal modulation (B5) was found as a unique self-similar solution of the Whitham-NLSE equations satisfying the plane wave conditions at infinity.

Solution (B4), (B5) describes a symmetric expanding oscillatory structure having the form of the fundamental soliton ( $m = 1$ ) resting at  $x = 0$ , and degenerating, via the modulated elliptic regime, into a vanishing amplitude linear wave ( $m = 0$ ) at the edges propagating away with the velocities  $\pm 2\sqrt{2}q_0$ . Importantly, modulation solution (B5) depends only on the plane wave background  $q_0$  and does not depend on the shape or amplitude of the initial perturbation  $\delta(x)$  and is, therefore, universal [27, 28].

Using the transformations (B2) we find the location of the expansion wedge in the physical  $t$ - $z$  plane:  $t_{\pm} = \pm 2\sqrt{2}\beta_2\gamma P_0 z$ .

The evolution of a localized initial perturbation towards the universal asymptotic pattern described by (B4), (B5) is shown in Fig. 4. In the experiment reported in Fig. 2 the initial stage of the evolution is robustly captured.

Remarkably, solution (B4), (B5) considered for  $x < 0$  ( $x > 0$ ) and complemented by  $q = 0$  for  $x > 0$  ( $x < 0$ ) also describes (up to the initial phase  $x_0$ ) the leading order term in the asymptotic solution of the 1D-NLSE *focusing dam break problem* [15, 31, 32]

$$q(x, 0) = q_{\pm}(x) = \begin{cases} q_0 & \text{for } \pm x < 0, \\ 0 & \text{for } \pm x > 0. \end{cases} \quad (\text{B6})$$

(the ‘ $\pm$ ’ refers to the two possible dam break configurations with ‘step down’ (+) and ‘step up’ (-)) The long time asymptotic solutions of (B1), (B6) are then given by  $q(x, t) = Q_{\pm}(x, \tau) + O(1/\sqrt{\tau})$  with

$$Q_{\pm}(x, \tau) = \begin{cases} Q(x, \tau) & \text{for } \pm x < 0, \\ 0 & \text{for } \pm x > 0. \end{cases} \quad (\text{B7})$$

and the modulation (B5) with the appropriate  $\sigma$  chosen. We note that the rigorous analysis of ref. [32] was performed for *decaying* initial conditions in the form of a rectangular barrier of the width  $L$  so the solution (B7), (B4), (B5) is rigorously valid as the leading term of the *small-dispersion* ( $\varepsilon \ll 1$ ) asymptotic  $q = Q(x, \tau) + O(\varepsilon^{1/2})$  for  $0 < \tau < L/4\sqrt{2}q_0$ .

One can see now that the leading term of the asymptotic solution for the locally perturbed plane wave is

equivalent to the leading term of the solution to the ‘double dam break’ problem,

$$Q(x, \tau) = Q_{-}(x, \tau) + Q_{+}(x, \tau).$$

We note that within the Whitham modulation theory the validity of essentially the same solution (B4), (B5) for both the locally perturbed plane wave and the dam break data is due to self-similarity of both problems on the level of modulation equations. The modulation self-similarity argument also explains persistence of the same universal pattern reported in [33] beyond the integrable 1D-NLSE. Indeed, the Whitham modulation theory does not have integrability of the original dispersive equation as a pre-requisite hence self-similar modulation solutions are in principle available for non-integrable systems [53].

### Appendix C: Influence of linear damping on the space-time evolution of the localized perturbations

In this section, we use numerical simulations of Eq. (1) to give clear evidence of the role of linear damping (unavoidable in the experiment) on the development of the nonlinear oscillatory structure that grows from the initial localized perturbation. If the loss term  $\alpha_{eff}$  in Eq. (1) is set to zero, Fig. 5(a) and 5(c) show that the nonlinear oscillatory structure expands linearly with the propagation distance inside the fiber. The edges of the nonlinear oscillating structure coincide well with the boundaries predicted by the asymptotic (long-time) theory, in full agreement with theoretical results reported in ref. [27–29]. These boundaries are given by  $t_{\pm} = \pm 2\sqrt{2}\beta_2\gamma P_0 z$  (see Appendix B) and they are plotted with white lines in Fig. 5.

The expansion of the nonlinear structure is strongly influenced by the presence of small linear dissipation, as shown in space-time diagrams of Fig. 5(b) and 5(d) that have been computed with  $\alpha_{eff} \neq 0$ . Even though the oscillatory structure is effectively located within the linear boundaries (white lines in Fig. 5(b) and 5(d)), the edges of the nonlinear oscillating structure are relatively far from the boundaries predicted by the asymptotic (long-time) theory, in particular for the initial condition where the localized perturbation is bright at initial time (Fig. 5(b)). The importance of weak linear fiber losses has already been pointed out in the experiments of ref. [34] where the dispersive dam-break flow of a photon fluid (defocusing regime) has been observed. Further theoretical work is needed to take into account the influence of a small linear damping term on the mathematical expression giving the boundaries separating the oscillatory region from the plane wave region.

[1] T. B. Benjamin and J. E. Feir, *Journal of Fluid Mechanics* **27**, 417 (1967).

[2] T. B. Benjamin, *Proceedings of the Royal Society of London A: Mathematical, Physical and Engineering Sciences*

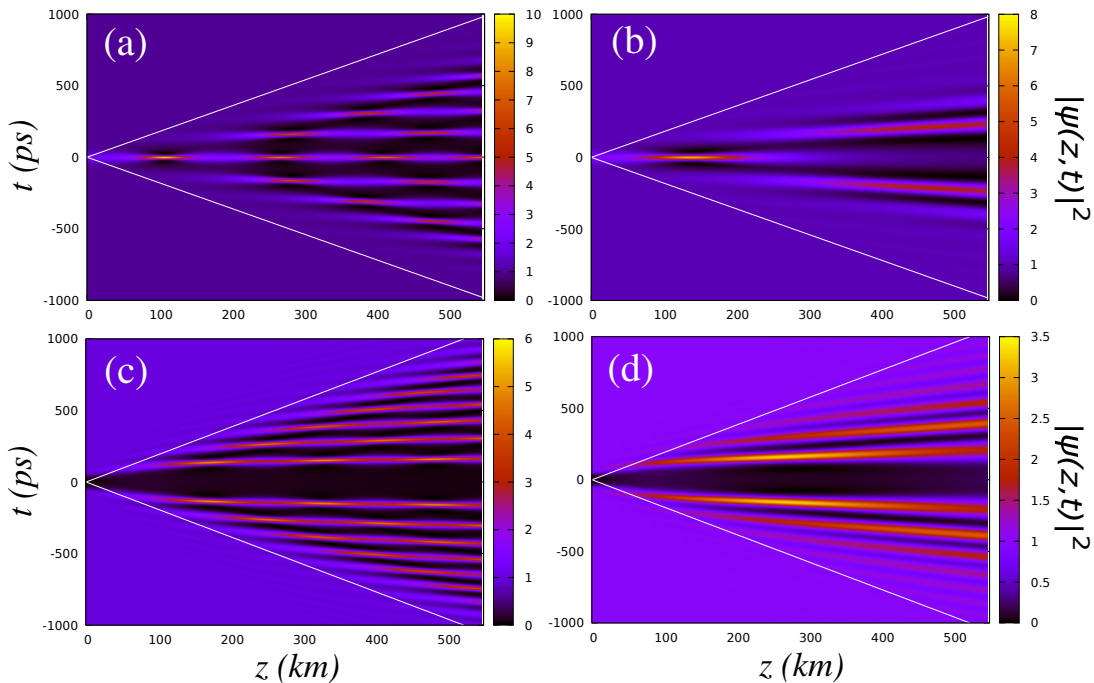


FIG. 5: Numerical simulations Eq. (1) showing the influence of a small linear damping term on the development of the nonlinear oscillatory structure while starting from (a), (b) a bright (positive) perturbation and (c), (d) a dark (negative) perturbation. The numerical simulations are made with the following parameters:  $\beta_2 = -22 \text{ ps}^2\text{km}^{-1}$ ,  $\gamma = 1.3\text{W}^{-1}\text{km}^{-1}$ . In (a) and (c),  $\alpha_{eff} = 0$  whereas in (b)  $\alpha_{eff} = 4.2 \times 10^{-3} \text{ km}^{-1}$  and in (d)  $\alpha_{eff} = 4 \times 10^{-3} \text{ km}^{-1}$ . In (a), (b), the initial condition is  $\psi(z = 0, t) = \sqrt{P_0(1 + \exp(-t/T_0)^2)}$  with  $P_0 = 14 \text{ mW}$ ,  $T_0 = 30\text{ps}$ . In (c), (d), the initial condition is  $\psi(z = 0, t) = \sqrt{P_0(1 - \beta \exp(-t/T_0)^4)}$  with  $P_0 = 16 \text{ mW}$ ,  $T_0 = 50 \text{ ps}$ ,  $\beta = 0.93$ .

- 299**, 59 (1967).
- [3] L. I. Zagryadskaya and L. A. Ostrovskii, Radiophysics and Quantum Electronics **11**, 548 (1968).
- [4] L. A. Ostrovskii and L. V. Soustov, Radiophysics and Quantum Electronics **15**, 182 (1972).
- [5] V. Zakharov and L. Ostrovsky, Physica D: Nonlinear Phenomena **238**, 540 (2009).
- [6] K. Tai, A. Hasegawa, and A. Tomita, Phys. Rev. Lett. **56**, 135 (1986).
- [7] M. Soljagic, M. Segev, T. Coskun, D. N. Christodoulides, and A. Vishwanath, Phys. Rev. Lett. **84**, 467 (2000).
- [8] D. R. Solli, G. Herink, B. Jalali, and C. Ropers, Nature Photonics **6**, 463 (2012).
- [9] J. Meier, G. I. Stegeman, D. N. Christodoulides, Y. Silberberg, R. Morandotti, H. Yang, G. Salamo, M. Sorel, and J. S. Aitchison, Phys. Rev. Lett. **92**, 163902 (2004).
- [10] M. Erkintalo, K. Hammani, B. Kibler, C. Finot, N. Akhmediev, J. M. Dudley, and G. Genty, Phys. Rev. Lett. **107**, 253901 (2011).
- [11] B. Kibler, J. Fatome, C. Finot, G. Millot, F. Dias, G. Genty, N. Akhmediev, and J. M. Dudley, Nature Physics **6**, 790 (2010).
- [12] B. Frisquet, B. Kibler, and G. Millot, Phys. Rev. X **3**, 041032 (2013).
- [13] N. Akhmediev and A. Ankiewicz, Phys. Rev. E **83**, 046603 (2011).
- [14] G. Biondini and E. Fagerstrom, SIAM J. Appl. Math. **75**, 136 (2015).
- [15] G. A. El, E. G. Khamis, and A. Tovbis, Nonlinearity **29**, 2798 (2016).
- [16] S. Coulibaly, E. Louvergneaux, M. Taki, and L. Brevdo, The European Physical Journal D **69**, 186 (2015).
- [17] B. Frisquet, B. Kibler, J. Fatome, P. Morin, F. Baronio, M. Conforti, G. Millot, and S. Wabnitz, Phys. Rev. A **92**, 053854 (2015).
- [18] O. Kimmoun, H. Hsu, H. Branger, M. Li, Y. Chen, C. Kharif, M. Onorato, E. Kelleher, B. Kibler, N. Akhmediev, et al., Scientific reports **6**, 28516 (2016).
- [19] A. Mussot, C. Naveau, M. Conforti, A. Kudlinski, F. Copie, P. Szriftgiser, and S. Trillo, Nature Photonics (2018).
- [20] J. M. Dudley, F. Dias, M. Erkintalo, and G. Genty, Nature Photonics **8**, 755 (2014).
- [21] J. M. Soto-Crespo, N. Devine, and N. Akhmediev, Phys. Rev. Lett. **116**, 103901 (2016).
- [22] V. Shrira and V. Geogjaev, J. Eng. Math. **67**, 11 (2010).
- [23] M. Onorato, S. Residori, U. Bortolozzo, A. Montina, and F. Arecchi, Phys. Rep. **528**, 47 (2013).
- [24] V. E. Zakharov and A. A. Gelash, Phys. Rev. Lett. **111**, 054101 (2013).
- [25] A. A. Gelash and V. E. Zakharov, Nonlinearity **27**, R1 (2014).
- [26] B. Kibler, A. Chabchoub, A. Gelash, N. Akhmediev, and V. E. Zakharov, Phys. Rev. X **5**, 041026 (2015).
- [27] G. Biondini and D. Mantzavinos, Phys. Rev. Lett. **116**, 043902 (2016).
- [28] G. Biondini, S. Li, and D. Mantzavinos, Physical Review E **94**, 060201 (2016).
- [29] G. El, A. Gurevich, V. Khodorovskii, and A. Krylov, Physics Letters A **177**, 357 (1993).



- [30] G. B. Whitham, *Linear and nonlinear waves*, vol. 42 (John Wiley & Sons, 2011).
- [31] A. Kamchatnov, *Physics Reports* **286**, 199 (1997).
- [32] R. Jenkins and K. D. McLaughlin, *Comm. Pure Appl. Math.* **67**, 246 (2014).
- [33] G. Biondini, S. Li, D. Mantzavinos, and S. Trillo, arXiv preprint arXiv:1710.05068 (2017).
- [34] G. Xu, M. Conforti, A. Kudlinski, A. Mussot, and S. Trillo, *Phys. Rev. Lett.* **118**, 254101 (2017).
- [35] P. Walczak, S. Randoux, and P. Suret, *Phys. Rev. Lett.* **114**, 143903 (2015).
- [36] P. Suret, R. El Koussaifi, A. Tikan, C. Evain, S. Randoux, C. Szwaj, and S. Bielawski, *Nature Communications* **7**, 13136 (2016).
- [37] M. Närhi, B. Wetzell, C. Billet, S. Toenger, T. Sylvestre, J.-M. Merolla, R. Morandotti, F. Dias, G. Genty, and J. M. Dudley, *Nature Communications* **7**, 13675 (2016).
- [38] A. Tikan, C. Billet, G. El, A. Tovbis, M. Bertola, T. Sylvestre, F. Gustave, S. Randoux, G. Genty, P. Suret, et al., *Phys. Rev. Lett.* **119**, 033901 (2017).
- [39] M. Tsang, D. Psaltis, and F. G. Omenetto, *Opt. Lett.* **28**, 1873 (2003).
- [40] A. Tikan, S. Bielawski, C. Szwaj, S. Randoux, and P. Suret, *Nature Photonics* **12**, 228 (2018).
- [41] E. Desurvire, M. Dignonnet, and H. J. Shaw, *Opt. Lett.* **10**, 83 (1985).
- [42] L. F. Mollenauer and K. Smith, *Opt. Lett.* **13**, 675 (1988).
- [43] M. Nakazawa, E. Yamada, H. Kubota, and K. Suzuki, *Electronics Letters* **27**, 1270 (1991).
- [44] A. G. Okhrimchuk, G. Onishchukov, and F. Lederer, *J. Lightwave Technol.* **19**, 837 (2001).
- [45] E. A. Golovchenko, J. M. Jacob, A. N. Pilipetskii, C. R. Menyuk, and G. M. Carter, *Opt. Lett.* **22**, 289 (1997).
- [46] F. Leo, S. Coen, P. Kockaert, S.-P. Gorza, P. Emplit, and M. Haelterman, *Nature Photonics* **4**, 471 (2010).
- [47] F. Copie, M. Conforti, A. Kudlinski, A. Mussot, and S. Trillo, *Phys. Rev. Lett.* **116**, 143901 (2016).
- [48] M. Taki, A. Mussot, A. Kudlinski, E. Louvergneaux, M. Kolobov, and M. Douay, *Physics Letters A* **374**, 691 (2010).
- [49] V. E. Zakharov, *Stud. Appl. Math.* **122**, 219 (2009).
- [50] S. Randoux, F. Gustave, P. Suret, and G. El, *Phys. Rev. Lett.* **118**, 233901 (2017).
- [51] G. A. El and A. M. Kamchatnov, *Phys. Rev. Lett.* **95**, 204101 (2005).
- [52] A. A. Gelash and D. S. Agafontsev, arXiv preprint arXiv:1804.00652 (2018).
- [53] G. El, *Chaos* **15**, 037103 (2005).